

Modelling Of An Ensemble Averaged Electric Arc In A Laboratory-Scale Electric Arc Furnace

Sergey Semenov¹, Patrick Namy¹, Magnus Sievers², Bernd Friedrich²

1. SIMTEC, Grenoble, France.

2. IME Process Metallurgy and Metal Recycling, RWTH Aachen University, Aachen, Germany.

Abstract

This work, which is done in the framework of the SisAl Pilot EU project, presents the use of COMSOL Multiphysics® for simulating an ensemble averaged electric arc in a laboratory-scale electric arc furnace. The SisAl Pilot project aims at optimising the silicon production in Europe by recycling materials and using a carbon-emission friendly technology. The silicon production experiments are conducted on laboratory and pilot scales in different types of furnaces, including electric arc furnaces (EAF). Besides experimental work, the process optimisation also relies on the numerical modelling. The present model simulates the furnace preheating and the initial slag melting in a laboratory-scale EAF, in which a DC electric arc operates between a graphite cathode and the anode formed by a thin layer of slag at the bottom of the graphite crucible. The main difficulty is associated with modelling the heat source due to the electric arc operation. There are various complex physical processes involved in the arc, including the plasma physics, induced high-velocity gas flow, and radiant and convective heat transfer towards the electrodes and the crucible. The channel-arc model is a commonly used approach for a simplified 0D simulation of the electric arc behaviour in a variety of applications. Being used in this model, it estimates the temperature and gas velocity in the arc column. At each moment in time, this 0D model provides an instantaneous spatial distribution of heat sources in the furnace relative to an immediate arc position. Additional modelling complication stems from the fact that the instantaneous electric arc is constantly changing its position on a very short time scale by jumping from one place to another. On average, it occupies the whole space under the graphite cathode. Thus, an ensemble averaging of the arc position is performed to obtain integral expressions of the averaged arc radiation and of the averaged Lorentz force that drives the gas flow in the plasma region. These integrals are evaluated in part analytically, and in part numerically. The experimentally measured electric potential difference and dissipated power are used as model input parameters. The following COMSOL® modules are employed in this model: Heat Transfer in Solids and Fluids with phase change, Turbulent Flow k - ϵ model in gas and liquid slag phases, Surface-to-Surface Radiation, Electric Currents to simulate the Joule effect in electrically conducting materials, Deformed Geometry to simulate variable electric arc shape, and Global and Domain ODEs to compute quantities associated with the ensemble averaging of the electric arc. A bidirectional coupling of all the modules is present due to multiple interdependencies. The averaging of the arc position helps to deconcentrate and redistribute heat sources, which results in plausible material temperatures and demonstrates the expected initial slag melting. The model can be further used to optimize furnace operation in terms of predicting possible thermal damages or heat losses and increasing the raw material melting efficiency. The presented ensemble averaging approach can be applied to other electric arc problems with a similar geometry.

Keywords: Electric Arc Furnace, Channel-Arc model, Ensemble averaging.

1. Introduction

This work is done in the framework of the SisAl Pilot EU project, which is focussed on demonstrating the possibility of metallurgical grade silicon production at pilot scale based on aluminothermic reduction of silica. In comparison with the traditional carbothermic reduction of silica, the advantage of the proposed technology is in its low CO₂ emission. As part of the project, the numerical modelling support of experimental works is stipulated. One of the modelling efforts is focussed on developing a numerical model of an existing laboratory-scale direct current (DC) electric arc furnace (EAF) used for the slag melting in the framework of the project. Developing a scalable numerical model of an electric arc is needed for the modelling of electric arc furnaces at both laboratory and pilot scales. Thus, the aim of the work is to create a mathematical model of an ensemble averaged electric arc, which could help

us to model more accurately the distributed heat source generated by the arc inside of the furnace and to achieve plausible in-furnace temperatures. The numerical model of the furnace will help us to estimate heat losses and to optimise the furnace efficiency for the slag making process.

In section 2, experimental and numerical methods are described. Sections 3 and 4 present governing equation and material properties. In section 5, numerical results are presented. Section 6 discusses the results and compares them with experimental data. Section 7 presents the conclusions of the work.

2. Experimental and numerical methods

2.1. Experimental methods

The experiments are performed at RWTH Aachen University in a laboratory-scale electric arc furnace that consists of a graphite crucible, alumina refractory and steel shell, see Figure 1. There is no dedicated furnace lid, but there is a removable metal

plate as part of the off-gas system, which is not shown in Figure 1 and is not modelled numerically. This type of furnaces is usually used in steel scrap recycling, production of silicon and ferroalloys or slag cleaning processes. In the framework of the SisAl Pilot project this furnace is used to carry out slag making and aluminothermic reduction trials. An additional refractory mat is placed between the crucible and the alumina refractory for a better thermal insulation. The bottom copper electrode is water cooled to keep its temperature below 700°C, though water temperature is not measured. Graphite powder is placed between the bottom electrode and the crucible. Thanks to its porosity, its thermal and electrical conductivities are lower than those of the graphite crucible, which increases Joule heat production under the crucible and reduces heat losses by conduction.

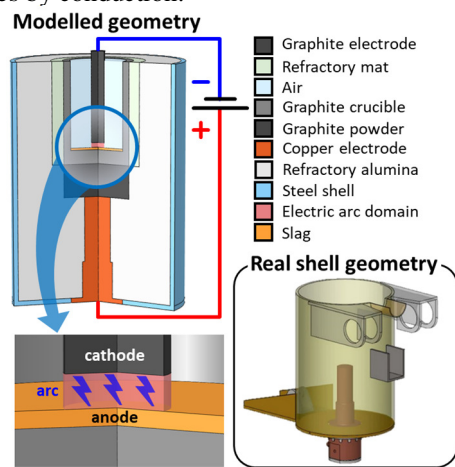


Figure 1. Real and modelled furnace geometry.

Furnace preheating is done by putting some graphite pieces into the graphite crucible and igniting an electric arc between the graphite top electrode and the graphite pieces. The slag making process starts by melting a small amount of raw material (51 wt.% CaO, 49 wt.% SiO₂) placed directly under the electric arc. When a paddle of melt forms, it spreads from the arc region towards crucible walls, where it loses heat and partially solidifies. More raw material is gradually added to increase the pool depth. The distance between the electrode and the melt, which corresponds to the length of the electric arc column, is difficult to measure, but it is known to be of the order of few millimetres. As soon as the depth of the melt becomes sufficient, the graphite electrode is submerged 1 to 3 cm into the molten material, and the heating continues in the mode of a submerged arc furnace (SAF), which significantly reduces material fuming. The input electric power is controlled by the furnace operator and can vary during the experiment. The slag melting process starts with 8-10 kW power. Once melting pool is formed, the input power is lowered to 4-7 kW. The typical voltage during open arc operation is 30-35 V. In-furnace temperature is measured with a pyrometer and ranges between 1600 and 1800 °C. The external shell temperature, which is measured after several hours of operation, is

115 °C in the upper section, 85 °C in the mid-section, and 40 °C in the lower section of the furnace. These temperatures will be used for the model validation.

2.2. Numerical methods

To reduce problem dimensionality, an assumption of axial symmetry is made (Figure 1): the pouring spout and other external structural elements are not modelled. For simplicity, a 5 mm slag layer is always present in the simulation. The distance between the graphite electrode and the slag layer is initially set to 10 mm and then adjusted alongside with the input power to fit the experimentally measured voltage drop of 30-35 V across the furnace terminals, and the available temperature measurements. Other adjustable parameters of the model, which are difficult to measure in experiments, are the thermal and the electrical conductivity of the graphite powder. The numerical model is developed within COMSOL Multiphysics® software, version 5.6, which is based on the finite element method. The following COMSOL® modules are employed in this model: Heat Transfer in Solids and Fluids with phase change, Turbulent Flow $k-\epsilon$ model in gas and liquid slag phases, Surface-to-Surface Radiation, Electric Currents to simulate the Joule effect in electrically conducting materials, Deformed Geometry to simulate variable electric arc shape, and Global and Domain ODEs to compute quantities associated with the ensemble averaging of the electric arc. A bidirectional coupling of all the modules is present due to multiple interdependencies. The heat losses towards outside include an empirical boundary condition for the external natural convection in the surrounding air, losses towards water-cooled bottom

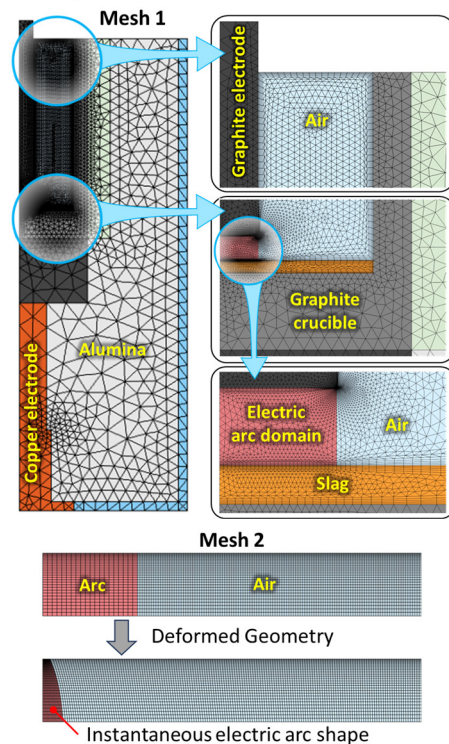


Figure 2. Spatial discretization meshes.

copper electrode, and thermal radiation towards ambient environment. The experimentally measured input power of 4-7 kW will be used as a model input parameter. The principal computational domain is spatially discretized with 13204 elements, see mesh 1 in Figure 2. Auxiliary rectangular domain and mesh 2 with 3600 elements are employed to model the instantaneous electric arc shape, see Figure 2, and to compute the associated instantaneous fields: the electric current density, the magnetic field, and the Lorentz force. Linear Lagrange elements are used for all physics modules, except for the Turbulent Flow in air, where, for a better numerical stability and convergence, quadratic elements are used for velocity and turbulent fields, while linear elements are used for pressure. The model with 113487 degrees of freedom is computed on a laptop with 8 physical cores Intel processor, 64 GB RAM, and an AMD Threadripper 5995WX Pro workstation with 1 TB RAM.

3. Governing Equations

3.1. Channel-arc model

The channel-arc model by Saevarsdottir et al. [1] is used to model an instantaneous direct current electric arc at each time moment during the time-dependent furnace simulation. In this model, for a given electric current I , a 0D steady-state equation for the arc temperature T_a is solved numerically by equilibrating the electrical power P_a dissipated by the arc with the power loss due to convection P_{conv} , electron flow P_{elec} and thermal arc radiation P_{rad} :

$$P_a = P_{conv} + P_{elec} + P_{rad} \quad (1)$$

$$P_a = I \cdot U_a$$

$$P_{conv} = \pi R_a^2 \rho_a v_{a,max} \cdot 7R / (2M_a) \cdot (T_a - T_{in})$$

$$P_{elec} = I \cdot [\varphi_{an} + U_{an} + (5/2) \cdot k_B T_a / e]$$

$$P_{rad} = \pi R_a^2 H Q_{rad}(T_a)$$

where

$$U_a = HI / [\pi R_a^2 \sigma_a(T_a)] + U_{ca} + U_{an}$$

$$v_{a,max} = I / (\pi R_a) \cdot \sqrt{\mu_0 \cdot (R_a^2 / R_{ca}^2 - 1) / (2\rho_a)}$$

$$R_{ca} = \sqrt{I / (\pi j_k)}, \quad j_k \approx 3.5 \times 10^7 \text{ A/m}^2$$

H is the arc height (distance between the slag and the graphite electrode surfaces), U_a is the voltage drop between the slag and the graphite electrode, ρ_a is the arc (air plasma) density, R is the universal gas constant, M_a is the air molar mass, T_{in} is the temperature of air that inflows into the arc column, $v_{a,max}$ is an estimate of the maximum instantaneous flow velocity in the arc column, k_B is the Boltzmann constant, $\varphi_{an} = 4.75 \text{ V}$ is the work function of the anode material [1], $U_{an} = 5 \text{ V}$ and $U_{ca} = 5 \text{ V}$ are the voltage drops in correspondingly the near-anode and the near-cathode regions [1], e is the electron charge, $Q_{rad}(T_a)$ is the volume density of the radiated power (in W/m^3), $\sigma_a(T_a)$ is the electrical conductivity of the air plasma, μ_0 is the vacuum permeability, R_{ca} is the cathode spot radius, and j_k is the mean current density at the cathode spot, which is governed by the thermionic emission, described by the Richardson-Dushman equation [2]. According to Bowman [3],

the mean value of j_k for DC arc furnaces is $3.5 \times 10^7 \text{ A/m}^2$. The average arc radius R_a is computed through the arc's volume V_a and height H :

$$R_a = \sqrt{V_a / (\pi H)}, \quad V_a = \int_0^H \pi R_{arc}^2(L_{arc}) dL_{arc}$$

where R_{arc} is given by the Bowman model [3]:

$$R_{arc}(L_{arc}) = R_{ca} (3.2 - 2.2 \cdot \exp[-L_{arc} / (5R_{ca})])$$

Solving equation (1) gives the arc temperature T_a , its electrical conductivity $\sigma_a(T_a)$, volume density of radiated power $Q_{rad}(T_a)$, and the instantaneous arc shape, which are further used in the model. The computation of current I is clarified in section 3.4.2.

3.2. Thermal radiation of an electric arc

Even though the channel-arc model [1] is essentially a 0D model, it presumes non-zero dimensions of the arc with some preselected spatial distributions of temperature T_a , electric current density, and vertical velocity v_a . In this work, uniform fields are assumed.

3.2.1. Instantaneous slag and crucible irradiance

To compute the instantaneous irradiances of slag (s), electrode (e), and crucible (c) due to arc radiation, we treat the arc column as a cylinder [1] of radius R_a located under the electrode centre, see Figure 3. We assume that arc is optically thin and does not absorb the radiation. Due to axial problem symmetry, all irradiances $G_{i,arc}$ ($i = s, e, c$) are axially symmetric. Due to vertical symmetry of the electrode and the slag surfaces with respect to the arc, their irradiances are identical functions of r : $G_{e,arc}(r) = G_{s,arc}(r)$. The crucible irradiance accounts for the electrode shadow with a shadow coefficient C_{sh} , see Figure 3:

$$G_{c,arc}^{sh} = G_{c,arc} \cdot C_{sh}$$

$$C_{sh} = \begin{cases} 1 & , z \leq H \\ (z_{sh} - z) / (z_{sh} - H) & , H < z \leq z_{sh} \\ 0 & , z > z_{sh} \end{cases}$$

where $G_{c,arc}$ is the crucible irradiance as if electrode was transparent, and $G_{c,arc}^{sh}$ is the one with shadow.

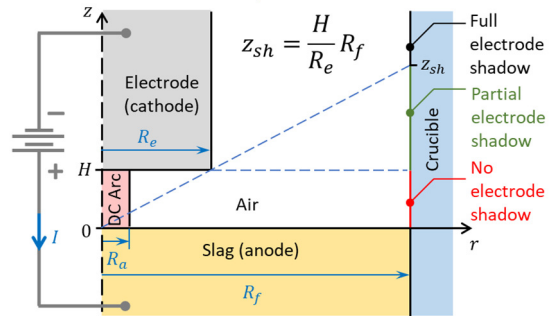


Figure 3. Problem geometry for computing instantaneous irradiances of slag, electrode, and crucible.

With the above assumptions, we can find the instantaneous slag irradiance $G_{s,arc}$ by integrating the arc radiation coming from each point of the arc column towards the slag surface at coordinate r :

$$G_{s,arc}(r) = \frac{Q_{rad}}{2\pi} \int_0^H \int_0^{R_a} \int_0^\pi \frac{z_a r_a d\varphi_a dr_a dz_a}{(r^2 + r_a^2 - 2r r_a \cos \varphi_a + z_a^2)^{3/2}}$$

Similarly, the crucible irradiance can be computed:

$$G_{c,arc}(z) = \frac{Q_{rad}}{2\pi} \int_0^H \int_0^{R_a} \int_0^\pi \frac{(R_f - r_a \cos \varphi_a) r_a d\varphi_a dr_a dz_a}{(R_f^2 + r_a^2 - 2R_f r_a \cos \varphi_a + (z_a - z)^2)^{3/2}}$$

The integration in both expressions is performed analytically with respect to r_a and z_a , and numerically with respect to φ_a with help of COMSOL® integration operators.

3.2.2. Averaged slag and crucible irradiance

Due to random walk motion of the cathode spot [4, 5], the electric arc changes its position under the electrode within very short time scales. To find the probability of its position, a simple random walk study has been performed. Accumulated statistics shows a uniform probability distribution of the arc position under the circular electrode surface.

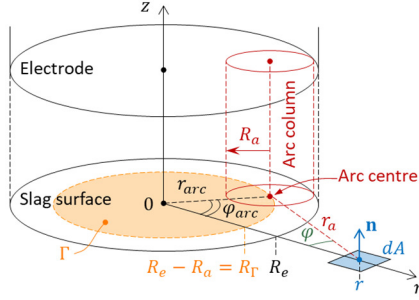


Figure 4. Geometry for the averaging of slag irradiance.

By combining the uniform probability of the arc position with the instantaneous irradiance $G_{s,arc}(r_a)$, where r_a is the radial distance from the area element dA to the instantaneous arc centre, see Figure 4, we obtain the statistically averaged slag irradiance:

$$G_{s,arc}^{av}(r) = \frac{1}{S_\Gamma} \int_\Gamma G_{s,arc}(r_a) dA_\Gamma$$

where $S_\Gamma = \pi R_\Gamma^2$ is the area of the circular region Γ of possible positions of the arc centre. The above integral is computed numerically. Thanks to the vertical problem symmetry, the averaged electrode irradiance $G_{e,arc}^{av}(r)$ is identical to $G_{s,arc}^{av}(r)$. For a proper statistical averaging of the instantaneous crucible irradiance $G_{c,arc}^{sh}(z)$, its precomputed numerical value must be corrected to be valid for any possible arc position (r_a, φ) , see Figure 4. The corrected value $G_{c,arc}^{sh,cor}(r_a, \varphi, z)$ is approximated by:

$$G_{c,arc}^{sh,cor}(r_a, \varphi, z) = G_{c,arc}^{cor}(r_a, \varphi, z) \cdot C_{sh}^{cor}(r_a, \varphi, z)$$

$$G_{c,arc}^{cor}(r_a, \varphi, z) = G_{c,arc}(z) \cdot C_G^{cor}(r_a, \varphi, z)$$

$$C_G^{cor}(r_a, \varphi, z) = \left(\frac{R_f^2 + (z - H/2)^2}{r_a^2 + (z - H/2)^2} \right)^{3/2} \cdot \frac{r_a}{R_f} \cos \varphi$$

$$C_{sh}^{cor}(r_a, \varphi, z) = \begin{cases} 1 & , 0 \leq z \leq H \\ (z_{sh}^{cor} - z)/(z_{sh}^{cor} - H) & , H < z \leq z_{sh}^{cor} \\ 0 & , z > z_{sh}^{cor} \end{cases}$$

$$z_{sh}^{cor} = H r_a / \left(r_a - R_f \cos \varphi + \sqrt{R_e^2 - R_f^2 \sin^2 \varphi} \right)$$

The statistically averaged crucible irradiance is then:

$$G_{c,arc}^{sh,av}(z) = \frac{1}{S_\Gamma} \int_\Gamma G_{c,arc}^{sh,cor}(r_a, \varphi, z) dA_\Gamma$$

The integration is done analytically with respect to φ and numerically with respect to r_a .

3.3. Averaged Lorentz force

The electric current density \mathbf{j} that passes through the instantaneous arc column creates a magnetic field \mathbf{B} and the volume density of the Lorentz force \mathbf{f}_L :

$$\mathbf{f}_L = \mathbf{j} \times \mathbf{B}$$

Given the arc's conductivity σ_a and shape, \mathbf{j} and \mathbf{B} can be computed numerically. A specific shape of the arc column is required for the appearance of the vertical component of the Lorentz force and of a directed plasma flow towards the slag surface: the arc column should have smaller diameter near the cathode (graphite electrode) and larger diameter near the anode (slag). In other words, the assumption of a cylindrical shape of the arc column, that was earlier used for the irradiance averaging, is no longer acceptable. Thus, in this section we assume a variable arc radius $R_{arc}(L_{arc})$ given by the Bowman model [3], see formula in section 3.1, where $L_{arc} = H - z$. Using the uniform probability of the arc position, the averaged Lorentz force is:

$$\mathbf{f}_L^{av}(r, z) = \frac{1}{S_\Gamma} \int_\Gamma \mathbf{f}_L(r_a, \varphi, z) dA_\Gamma$$

The integration is done analytically with respect to φ and numerically with respect to r_a .

3.4. Electric current equation

3.4.1. In an instantaneous electric arc

The current continuity equation is solved in an instantaneous electric arc:

$$\nabla \cdot \mathbf{j} = 0, \quad \mathbf{j} = -\sigma_a \nabla V$$

where \mathbf{j} is the electric current density, σ_a is the arc's electrical conductivity, and V is the electric potential. Since arc shape $R_{arc}(L_{arc})$ depends on the current I , an additional domain with a deformable geometry, see mesh 2 in Figure 2, is used to model its instantaneous shape and the electric current passing through it. The boundary condition of axial symmetry is imposed at $r = 0$. Electric insulation is on the arc-air interface: $\mathbf{j} \cdot \mathbf{n} = 0$. Uniform normal current density is on the arc-cathode and arc-anode interfaces. $V = 0$ at $(r = 0, z = H)$.

3.4.2. In the rest of the furnace

To find the total electric power P dissipated in the entire furnace, the current continuity equation is solved in all conducting parts of the furnace:

$$\nabla \cdot (-\sigma \nabla V) = 0$$

where σ is the electrical conductivity of materials. The electric arc domain is not included into this electrical model, since the voltage drop U_a across the arc has been already computed in the 0D channel-arc model. The axial symmetry condition is imposed at $r = 0$. Insulation on interfaces with non-conducting materials: $\mathbf{j} \cdot \mathbf{n} = 0$. Zero potential is at the top of the graphite electrode. Total current condition is at the bottom of the copper electrode: $\int_S \mathbf{j} \cdot \mathbf{n} dS = -I$. Uniform normal current density $\mathbf{j} \cdot \mathbf{n} = I/(\pi R_e^2)$ is imposed on the interfaces between the electric arc domain and the anode (slag) and cathode (graphite electrode). The electric potential difference between these interfaces is set to be equal to the arc voltage U_a . Resolving the above electric equation gives the voltage drop $U_f(I)$ across the entire furnace as function of current I that passes through it. This allows us to find the total dissipated electric power:

$$P = I \cdot U_f(I)$$

Since the furnace operates at a given value of the total electric power $P = P_0$, the following global constraint is employed to compute the current I :

$$I \cdot U_f(I) = P_0$$

3.5. Turbulent fluid dynamics

3.5.1. In the air domain

The action of the averaged Lorentz force in the electric arc domain results in a turbulent air flow that contributes to the electric arc power dissipation and to the heat transport towards the slag surface. The stationary incompressible RANS equations with k - ε turbulence model are solved in the air and in the averaged electric arc domains:

$$\begin{aligned} \rho(\mathbf{u} \cdot \nabla)\mathbf{u} &= \nabla \cdot [-p\mathbf{I} + \mathbf{K}] + \mathbf{f}_L^{av} \\ \nabla \cdot \mathbf{u} &= 0, \quad \mathbf{K} = (\mu + \mu_T)(\nabla\mathbf{u} + (\nabla\mathbf{u})^T) \\ \rho(\mathbf{u} \cdot \nabla)k &= \nabla \cdot [(\mu + \mu_T/\sigma_k)\nabla k] + P_k - \rho\varepsilon \\ \rho(\mathbf{u} \cdot \nabla)\varepsilon &= \nabla \cdot [(\mu + \mu_T/\sigma_\varepsilon)\nabla\varepsilon] + C_{\varepsilon 1}\frac{\varepsilon}{k}P_k - C_{\varepsilon 2}\rho\frac{\varepsilon^2}{k} \\ \mu_T &= \rho C_\mu k^2/\varepsilon, \quad P_k = \mu_T[\nabla\mathbf{u} : (\nabla\mathbf{u} + (\nabla\mathbf{u})^T)] \\ \sigma_k &= 1, \sigma_\varepsilon = 1.3, C_{\varepsilon 1} = 1.44, C_{\varepsilon 2} = 1.92, C_\mu = 0.09 \end{aligned}$$

Since slag is much more viscous than air, its velocity at the air-slag interface can be neglected with respect to the air velocity. Thus, the no-slip boundary condition is applied on all air interfaces with other materials. The axial symmetry is applied at $r = 0$. Pressure $p = 0$ is set in the corner of the air domain.

3.5.2. In the slag layer

The stationary incompressible RANS equations with k - ε turbulence model, like those solved in the air, are also solved in the slag domain. In the solid or porous part of the slag volume, the Darcy force \mathbf{f}_D is added:

$$\mathbf{f}_D = -\mu_s\mathbf{u}/K_{perm}$$

where μ_s is the slag viscosity and K_{perm} is the slag permeability (Kozeny-Carman model):

$$K_{perm} = K_0 g_l^3 / (1 - g_l)^2$$

where $K_0 = 7 \times 10^{-9} \text{ m}^2$ and g_l is liquid fraction. Additional source terms related to the Darcy force are also added into the turbulence equations [6]: $-2\mu_s k/K_{perm}$ in the k equation and $-2\mu_s \varepsilon/K_{perm}$ in the ε equation. Axial symmetry is imposed at $r = 0$. No-slip condition is applied at the slag-crucible interface. Zero normal velocity and tangential stress are applied at the slag-air interface:

$$\mathbf{u} \cdot \mathbf{n} = 0$$

$$\sigma_{\tau,slag} = \begin{cases} \sigma_{\tau,air}, & \text{if slag is liquid} \\ 0, & \text{if slag is solid} \end{cases}$$

where $\sigma_\tau = \boldsymbol{\sigma} - (\boldsymbol{\sigma} \cdot \mathbf{n})\mathbf{n}$, $\boldsymbol{\sigma} = [-p\mathbf{I} + \mathbf{K}] \cdot \mathbf{n}$. Pressure $p = 0$ is set in the corner of slag domain.

3.6. Heat transfer with surface-to-surface radiation

The following heat equation is solved in all domains:

$$\begin{aligned} \rho c_p' \left(\frac{\partial T}{\partial t} + \mathbf{u} \cdot \nabla T \right) + \nabla \cdot \mathbf{q} &= Q_{Joule} \\ \mathbf{q} &= -(\lambda + \lambda_T)\nabla T \\ \lambda_T &= c_p \mu_T / \text{Pr}_T, \quad \text{Pr}_T = 0.85 \end{aligned}$$

where T is temperature, ρ is density, \mathbf{q} is the conductive heat flux, λ and λ_T are respectively the molecular and the turbulent thermal conductivity, Pr_T is the turbulent Prandtl number, c_p' is the isobaric specific heat capacity modified with the Apparent

Heat Capacity method to account for phase changes, Q_{Joule} is the volume density of the Joule heat source:

$$Q_{Joule} = \begin{cases} P_{conv}/(\pi R_e^2 H), & \text{in the arc domain} \\ \sigma(\nabla V)^2, & \text{in other furnace parts} \end{cases}$$

In solids, including solid slag phase, the terms $(\mathbf{u} \cdot \nabla T)$ and λ_T are omitted. The power P_{elec} , dissipated by the electron flow, contributes to the heat source q_{elec} at the air-slag interface:

$$q_{elec} = \begin{cases} P_{elec}/(\pi R_e^2), & r \leq R_e \\ 0, & r > R_e \end{cases}$$

Another contribution to interfacial heat sources comes from surface-to-surface radiation:

$$\begin{aligned} q_{rad} &= \varepsilon(G_{rad} - \sigma_{SB}T^4) \\ G_{rad} &= G_{arc}^{av} + G_{rad}^{mutual} + G_{rad}^{ambient} \\ G_{arc}^{av} &= \begin{cases} G_{e,arc}^{av}(r), & \text{at the electrode surface} \\ G_{s,arc}^{av}(r), & \text{at the slag surface} \\ G_{c,arc}^{av}(z), & \text{at the crucible surface} \end{cases} \end{aligned}$$

where ε is the hemispherical emissivity of radiating surfaces and σ_{SB} is the Stefan-Boltzmann constant. Thus, the total heat source at the air-slag interface is:

$$(\mathbf{q}_{air} - \mathbf{q}_{slag}) \cdot \mathbf{n} = q_{elec} + q_{rad}$$

where unit normal vector \mathbf{n} points into air. On other surfaces that participate in the radiant heat exchange the contribution q_{elec} is zero. For the air gaps that are present between the refractory mat and surrounding materials, a linearized radiative heat exchange combined with the air heat conduction is applied:

$$\begin{aligned} \mathbf{q}_{rm} \cdot \mathbf{n}_{rm} &= \mathbf{q} \cdot \mathbf{n}_{rm} = h_{gap}(T_{rm} - T) \\ h_{gap} &= \lambda_{air}(\bar{T})/\Delta_{gap} + 2\sigma_{SB}\bar{T} \cdot (T^2 + T_{rm}^2) \\ \bar{T} &= (T + T_{rm})/2 \end{aligned}$$

where index rm stands for the refractory mat, unit normal vector \mathbf{n}_{rm} points into a neighbouring material, $\Delta_{gap} = 2 \text{ mm}$ is the gap size. Temperature and heat flux continuity are set on interfaces that do not participate in the radiant heat exchange:

$$T_{up} = T_{down}, \quad \mathbf{q}_{up} \cdot \mathbf{n} = \mathbf{q}_{down} \cdot \mathbf{n}$$

Ambient temperature T_{amb} is set at the bottom of the copper electrode, as it is water cooled. Convective heat flux is imposed on other external boundaries:

$$-\mathbf{n} \cdot \mathbf{q} = h(T_{amb} - T)$$

where \mathbf{n} is the outward unit normal vector and h is the heat transfer coefficient computed according to an empirical model of external natural convection. The initial furnace temperature equals T_{amb} .

4. Material properties

A single set of temperature-dependent graphite properties, found in literature [7, 8], is used for both the crucible and the top electrode, as well as for the graphite powder but with thermal and electrical conductivity multiplied by 0.1 to simulate the effect of its porosity. The structural steel and copper properties, available from the COMSOL® materials library, are used respectively for the steel shell and the copper electrode. The properties of the EKW-CAST I 1700-18 alumina, provided by the supplier, are used for refractory. The Fibermax® Matte U-410 DE properties are used for the refractory mat. Slag properties as functions of its composition and temperature are modelled with the Ken Mills model

[9]. Its viscosity is given by the Riboud model [9, 10], and density is by the Xin et al. [11] model. Air properties are those from the COMSOL® materials library, except for its viscosity and thermal conductivity that are modelled with the Sutherland's law [12]. Besides the turbulent conductivity $\lambda_{T,air}$ of air, its molecular conductivity λ_{air} is additionally enhanced in the arc domain with an empirical Nusselt number to account for the intensive mixing due to high instantaneous arc velocity. The plasma properties, such as volume density of radiated power Q_{rad} and the electrical conductivity σ_a are shown in Figure 5 as functions of the arc temperature T_a [2].

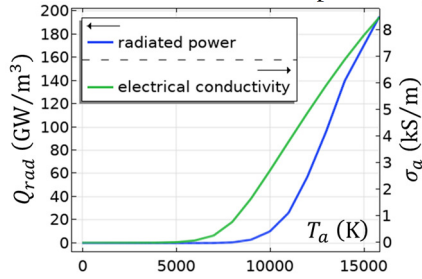


Figure 5. Plasma properties.

5. Numerical results

The below results are shown for the arc length $H = 4$ mm and furnace input powers P ranging from 3.5 to 7 kW. The computed temperature field is shown in Figure 6. After almost 3 hours of furnace operation, the process is not yet stationary, but the changes are already quite slow. Numerically, the initial slag layer is completely melted if $P \geq 6.3$ kW.

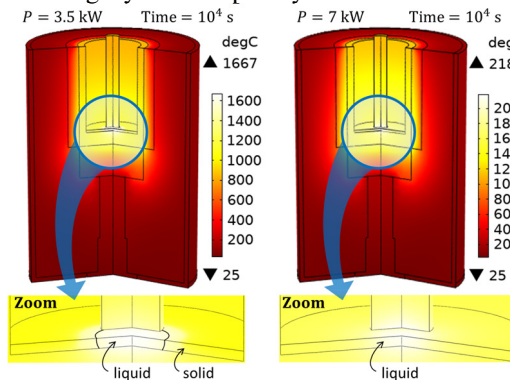


Figure 6. Computed temperature fields after 10^4 seconds of furnace operation at input powers of 3.5 and 7 kW.

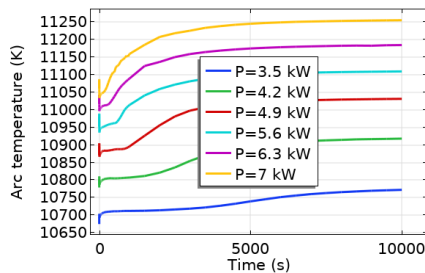


Figure 7. Electric arc temperature.

The time evolution of the instantaneous arc temperature $T_a(t)$ is shown in Figure 7. The instantaneous plasma velocity in the arc column varies from 137 to 185 m/s, while the plasma

conductivity is from 3.6 to 4.1 kS/m. The logarithm of the averaged irradiance $\log_{10}(G_{arc}^{av}/1[W/m^2])$ due to arc radiation is shown in Figure 8. The highest irradiance is at the centre of the slag surfaces, and ranges from 575 to 1660 kW/m² depending on P . Figure 9 shows the Reynolds averaged velocity field. The global enthalpy conservation is well satisfied, see Figure 10. Note that the numerically computed energy losses by radiation might be overestimated, because the off-gas system with its metal plate above the furnace is not modelled here.

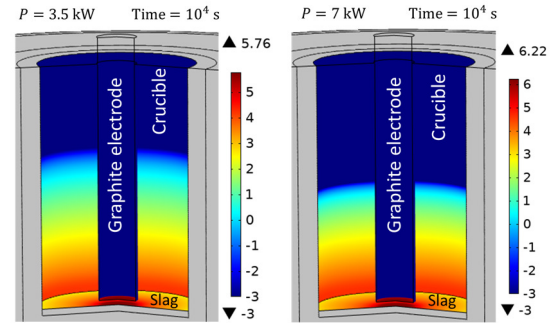


Figure 8. \log_{10} of the averaged irradiance of the graphite electrode, slag, and crucible due to arc radiation.

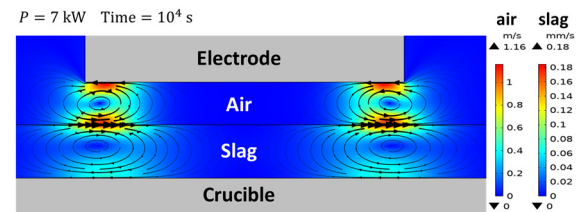


Figure 9. Reynolds averaged velocity field.

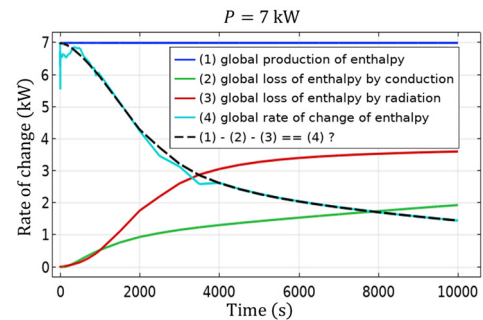


Figure 10. Global balance of enthalpy.

6. Discussion, comparison with experiments

The results of numerical simulations mostly depend on the arc length H and the furnace input power P . A parametric study on these two parameters is performed to fit the experimental data. Figure 11 shows the voltage drop U_f across the furnace as function of H and P . As P increases, U_f reduces due to decreasing resistance of the slag layer. Indeed, for a higher input power, the slag temperature, fraction of its liquid phase and its electrical conductivity are also higher. The model predicts U_f values similar to the experimental ones when $H \leq 4$ mm. The computed external shell temperature T is compared with the experimentally measured one, see Figure 12. As one can see, the shell temperature is mostly governed by the input power P , while the influence

of the arc length H is insignificant. By comparing numerical and experimental temperatures at the bottom ($z = -33$ cm) and in the middle ($z = -7$ cm) of the furnace shell, one can conclude that, in experiments, the long-term average input power over several hours of furnace operation must be around 3.5 kW. However, at the top of the furnace ($z = 19$ cm), there is a significant difference between the numerical temperature at $P = 3.5$ kW and the experimental one, which can be explained as follows. Since the off-gas system at the top of the furnace was not modelled, the simulated heat losses there could be overestimated, and, therefore, the simulated temperature T could be underestimated, which corresponds well to what we see in Figure 12. Regarding the liquid slag pool, the average simulated temperature on its surface is 1594 °C at $P = 3.5$ kW and 1716 °C at 7 kW, which falls within the range of experimentally measured melt temperatures.

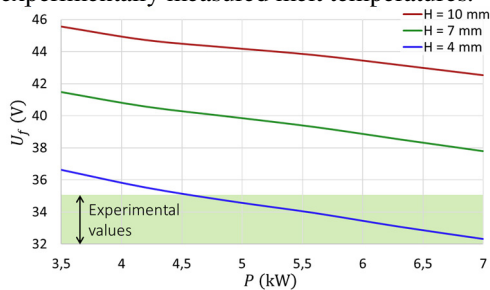


Figure 11. Voltage drop across the furnace terminals.

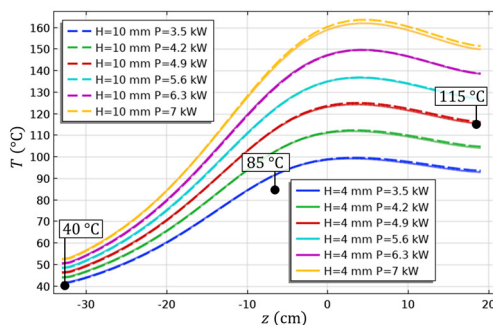


Figure 12. Computed (lines) and measured (markers) external shell temperature.

7. Conclusions

Within the adopted assumptions, the proposed numerical model has successfully simulated the preheating of the laboratory-scale electric arc furnace and the initial slag melting in it. The ensemble averaging of the channel-arc model is demonstrated to be an efficient approach for simulating a distributed heat source in the electric arc furnace, which results in plausible material temperatures in the neighbourhood of the electric arc. The work is validated against experimental data: taking arc length $H \leq 4$ mm and the average long-term input power $P = 3.5$ kW has resulted in a satisfactory fitting of experimental temperatures and voltage drops. The model has shown that for a complete melting of the initial slag layer, the initial input power should be above 6.3 kW, which is also confirmed in practice. The presented ensemble

averaging approach can be applied to other electric arc problems with a similar geometry.

References

- [1] G. A. Saevarsdottir, H. L. Larsen and J. A. Bakken, "Modelling of industrial ac-arcs. High Temperature Material Processes," *An International Quarterly of High-Technology Plasma Processes*, no. 3(1), 1999.
- [2] Q. G. Reynolds, *Mathematical and computational modelling of the dynamic behaviour of direct current plasma arcs*, PhD Thesis, University of Cape Town, 2009.
- [3] B. Bowman, "Properties of arcs in DC furnaces," in *Electric furnace conference proceedings*, 1994.
- [4] J. E. Daalder, "Random walk of cathode arc spots in vacuum," *Journal of Physics D: Applied Physics*, vol. 16, p. 17–27, 1983.
- [5] E. Hantzsche, B. Juttner and H. Pursch, "On the random walk of arc cathode spots in vacuum," *Journal of Physics D: Applied Physics*, vol. 16, p. L173–L179, 1983.
- [6] A. Jardy, *Modélisation mathématique et simulation numérique de procédé de refusion à l'arc sous vide*, 2005.
- [7] Entegris, Inc., *Properties and Characteristics of graphite, for the semiconductor industry.*, 2013.
- [8] D. McEligot, W. D. Swank, D. L. Cottle and F. I. Valentin, *Thermal properties of G-348 graphite*, Idaho Falls, ID (United States): Idaho National Lab. (INL), 2016.
- [9] K. C. Mills, L. Yuan and R. T. Jones, "Estimating the physical properties of slags.," *J. S. Afr. Inst. Min. Metall.*, vol. 111, no. 10, pp. 649–658, 2011.
- [10] G.-h. Zhang, Y.-l. Zhen and K.-c. Chou, "Viscosity and structure changes of CaO-SiO₂-Al₂O₃-CaF₂ melts with substituting Al₂O₃ for SiO₂," *Journal of Iron and Steel Research International*, vol. 23, no. 7, p. 633–637, 2016.
- [11] J. Xin, L. Gan, L. Jiao and C. Lai, "Accurate density calculation for molten slags in SiO₂-Al₂O₃-CaO-MgO systems," *ISIJ International*, vol. 57, no. 8, pp. 1340–1349, 2017.
- [12] COMSOL Documentation, "Sutherland's law," [Online]. Available: https://doc.comsol.com/5.5/doc/com.comsol.help.cfd/cfd_ug_fluidflow_high_mach.08.27.html.

Acknowledgements

Authors acknowledge the financial support under the Horizon 2020 European Union project SisAl Pilot, Grant Agreement N°869268.